Geochemistry Geophysics Geosystems G3

Article
Volume 00, Number 00
0 MONTH 2013
doi: 10.1002/ggge.20150
ISSN: 1525-2027

Published by AGU and the Geochemical Society

The P and S wave velocity structure of the mantle beneath eastern Africa and the African superplume anomaly

Gabriel D. Mulibo
Department of Geosciences, Pennsylvania State University, University Park, Pennsylvania, USA (gdm135@psu.edu)

Also at School of Earth Sciences and Engineering, Nelson Mandela-African Institute of Science and Technology, P.O Box 447, Arusha, Tanzania

Andrew A. Nyblade
Department of Geosciences, Pennsylvania State University, University Park, Pennsylvania, USA

[1] *P* and *S* relative arrival time residuals from teleseismic earthquakes recorded on over 60 temporary AfricaArray broadband seismic stations deployed in Uganda, Tanzania, and Zambia between 2007 and 2011 have been inverted, together with relative arrival time residuals from earthquakes recorded by previous deployments, for a tomographic image of mantle wave speed variations extending to a depth of 1200 km beneath eastern Africa. The image shows a low-wave speed anomaly (LWA) well developed at shallow depths (100–200 km) beneath the Eastern and Western branches of the Cenozoic East African rift system and northwestern Zambia, and a fast wave speed anomaly at depths $\leq$ 350 km beneath the central and northern parts of the East African Plateau and the eastern and central parts of Zambia. At depths $\geq$350 km the LWA is most prominent under the central and southern parts of the East African Plateau and dips to the southwest beneath northern Zambia, extending to a depth of at least 900 km. The amplitude of the LWA is consistent with a $\sim$150–300 K thermal perturbation, and its depth extent indicates that the African superplume, originally identified as a lower mantle anomaly, is likely a whole mantle structure. A superplume extending from the core-mantle boundary to the surface implies an origin for the Cenozoic extension, volcanism, and plateau uplift in eastern Africa rooted in the dynamics of the lower mantle.

Components: 9420 words, 11 figures.

Keywords: tomography; low-wave speed anomaly; eastern Africa; African superplume; Cenozoic rifting.

Index Terms: 7270 Tomography: Seismology; 6982 Tomography and imaging: Radio Science; 8180 Tomography: Tectonophysics

Received 20 February 2013; **Revised** 4 April 2013; **Accepted** 12 April 2013; **Published** 00 Month 2013.

Mulibo, G. D., and A. A. Nyblade (2013), The *P* and *S* wave velocity structure of the mantle beneath eastern Africa and the African superplume anomaly, *Geochem. Geophys. Geosyst., 14*, doi:10.1002/ggge.20150.

© 2013. American Geophysical Union. All Rights Reserved.

1. Introduction

[2] Since the early global tomographic models of the 1980s, many authors have remarked on the anomalous nature of the mantle beneath Africa [e.g., *Dziewonski*, 1984; *Dziewonski and Woodhouse*, 1987], which is characterized by a large low-wave speed anomaly (LWA) in the lower mantle commonly referred to as the African superplume [e.g., *Ritsema et al*., 1999, 2011; *Mégnin and Romanowicz*, 2000; *Ritsema and Allen*, 2003; *Zhao*, 2004; *Montelli et al*., 2006]. The structure of the African superplume, which is fundamental to understanding mantle convection, is not well understood. Most tomographic models show the LWA extending from the core-mantle boundary upward into the midmantle where it tilts toward the northeast beneath eastern Africa.

[3] The upward extent of the LWA, however, remains uncertain. Many global models show the LWA reaching depths of at least 1500 km [*Ritsema et al*., 1999, 2011; *Montelli et al*., 2006; *Simmons et al*., 2009, 2010, 2012], and *Hansen et al*. [2012] demonstrated that the LWA could extend to depths of $\leq$1100 km. But the limited vertical resolution in these models makes it difficult to determine if the LWA extends into the mantle transition zone and connects to anomalous upper mantle structure beneath eastern Africa. Regional studies of upper mantle structure in eastern Africa, on the other hand, have imaged a LWA extending from shallow depths downward into the transition zone but have not been able to ascertain if the anomaly continues through the transition zone to connect with the superplume structure in the lower mantle [e.g., *Ritsema et al*., 1998; *Owens et al*., 2000; *Weeraratne et al*., 2003; *Park and Nyblade*, 2006; *Huerta et al*., 2009; *Adams et al*., 2012].

[4] Determining if the African superplume extends from the core-mantle boundary under southern Africa to the surface beneath eastern Africa would not only place a first-order constraint on mantle dynamics, but also on geodynamic models for the origin of the Cenozoic rifting, volcanism and plateau uplift in eastern Africa. Three kinds of geodynamic models have been proposed. The first category of models invokes small-scale convection associated with edge flow [e.g., *King and Anderson*, 1995; *King and Ritsema*, 2000; *King*, 2007] or passive stretching of the lithosphere [e.g., *Buck*, 1986; *Mutter et al*., 1988]. The second type invokes one or more plumes with plume head material ponded beneath the lithosphere fed by a narrow ($\sim$100–200 km diameter) plume tail [e.g., *Green et al*., 1991; *Slack et al*., 1994; *Burke*, 1996; *Ebinger and Sleep*, 1998; *George et al*., 1998; *Nyblade et al*., 2000; *Chang and Van der Lee*, 2011]. And the third grouping of models attributes the Cenozoic tectonism to a superplume [e.g., *Hilton et al*., 2011; *Nyblade*, 2011; *Adams et al*., 2012; *Hansen et al*., 2012]. If the African superplume is a through-going mantle structure then the latter type of model is obviously favored.

[5] In this paper, we investigate mantle structure beneath eastern Africa using data sets obtained from several seismic networks in Uganda, Kenya, Tanzania, Malawi and Zambia. The large aperture provided by the combined networks enables us to image a region of the midmantle where existing tomography models suggest that the superplume structure may extend through the transition zone into the upper mantle. *P* and *S* wave relative arrival time residuals, obtained using a multichannel cross correlation technique, have been tomographically inverted for a 3-D image of mantle wave speeds. The 3-D image better resolves mantle structure beneath eastern Africa than previous models, enabling us to address further the question of whether or not the African superplume is a whole mantle structure.

2. Background and Previous Seismic Studies

2.1. Regional Geology and Tectonic Setting

[6] The Precambrian tectonic framework of eastern Africa is comprised of the Archean Tanzania Craton, which likely includes the Basement Complex of northern Uganda, the Paleoproterozoic Bangweulu Block, and several Proterozoic mobile belts [*Cahen et al*., 1984; *Begg et al*., 2009] (Figure 1). This framework has been affected by two primary episodes of rifting, first during the Karoo (Permian-Jurassic) caused by the breakup of Gondwana, and then in the Cenozoic. In eastern Africa, the Karoo rifts form an intracratonic, largely nonmagmatic system, with rift basins oriented northeast-southwest or northwest-southeast [e.g., *Catuneanu et al*., 2005].

[7] The Cenozoic rift system has two branches, the Western branch and the Eastern branch (Figure 1). The Western branch, stretching from northern Uganda to southern Malawi and central Mozambique, consists of several en echelon fault-bounded

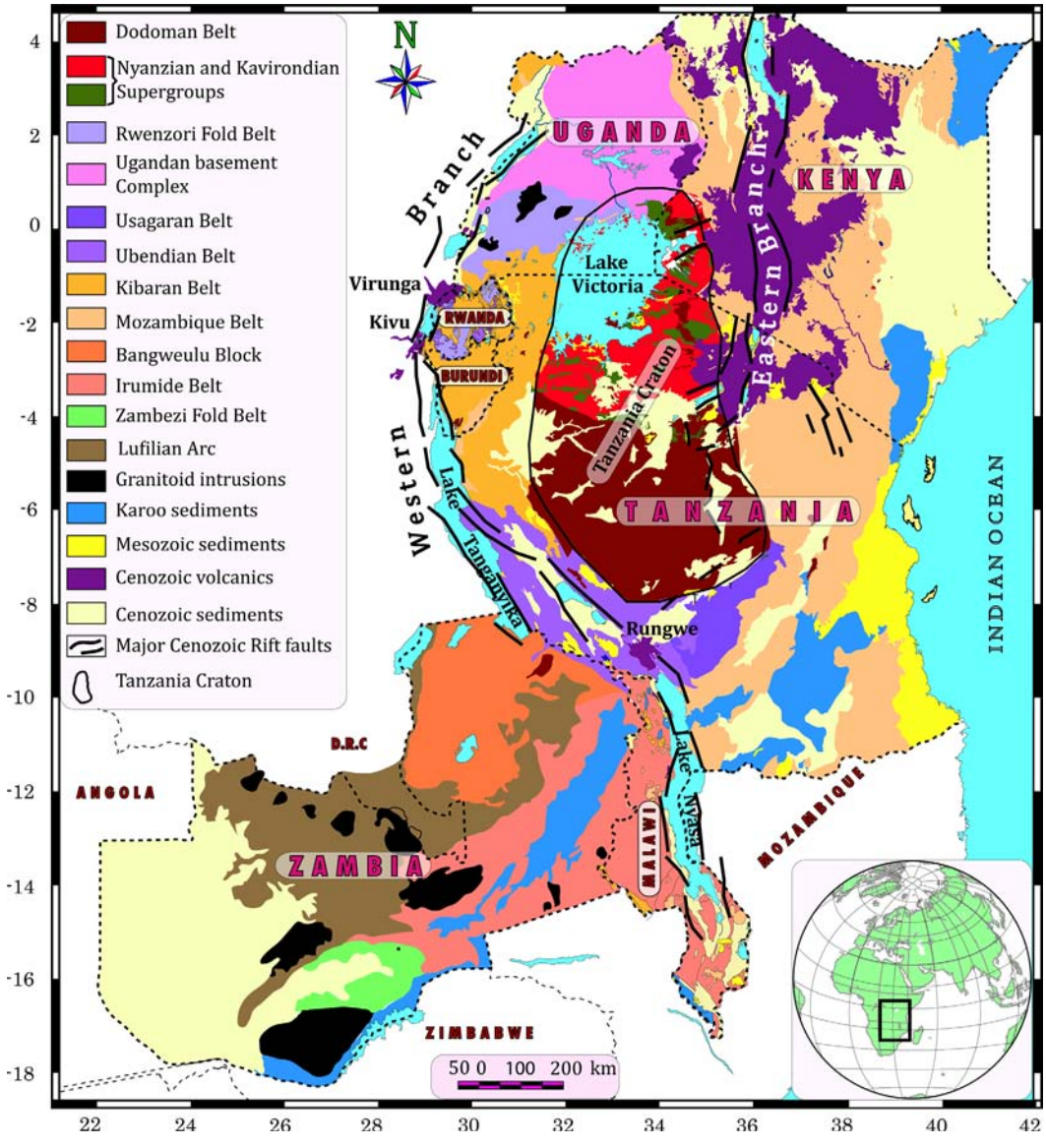


Figure 1. Map showing the main geologic and tectonic features of the study region. The map was modified from *Mathu and Davies* [1996], *Pinna et al*. [2004], and *De Waele et al*. [2008]. [Color figure can be viewed in the online issue, which is available at wileyonlinelibrary.com.]

rift basins within the Rwenzori, Kibaran, Ubendian, and Irumide mobile belts [*Ebinger et al*., 1989]. Some of the rift basins to the south and southwest of the Tanzania Craton have developed within or adjacent to Karoo rifts, resulting in the reactivation of Karoo-aged faults. The Eastern branch, mostly developed within the Mozambique Belt, extends from the Afar triple junction southward through Ethiopia, Kenya and Tanzania. In Kenya, the Eastern branch, locally referred to as the Kenya or Gregory rift, is narrow (50–80 km wide) but in northeastern Tanzania is characterized by a wider zone (300 km) of block faulting [*Dawson*, 1992; *Ebinger et al*., 1997; *Foster et al*., 1997].

[8] The Eastern branch of the rift system is volcanically more active than the Western branch, with magmatism covering most of the Kenya rift and parts of northern Tanzania. Magmatism initiated about 35–40 Ma in northern Kenya near Lake Turkana [*Macdonald et al*., 2001; *Furman et al*., 2006], ca. 30 Ma in other parts of northern Kenya [*Morley et al*., 1992], ca. 15 Ma in central Kenya, ca. 12 Ma in southern Kenya [*Morley et al*., 1992; *Mechie et al*., 1997] and at 8 Ma in northern Tanzania [*Dawson*, 1992; *Foster et al*., 1997]. The Western branch hosts a number of isolated volcanic centers including the Virunga, Kivu and Rungwe volcanic provinces [*Ebinger*, 1989]. The

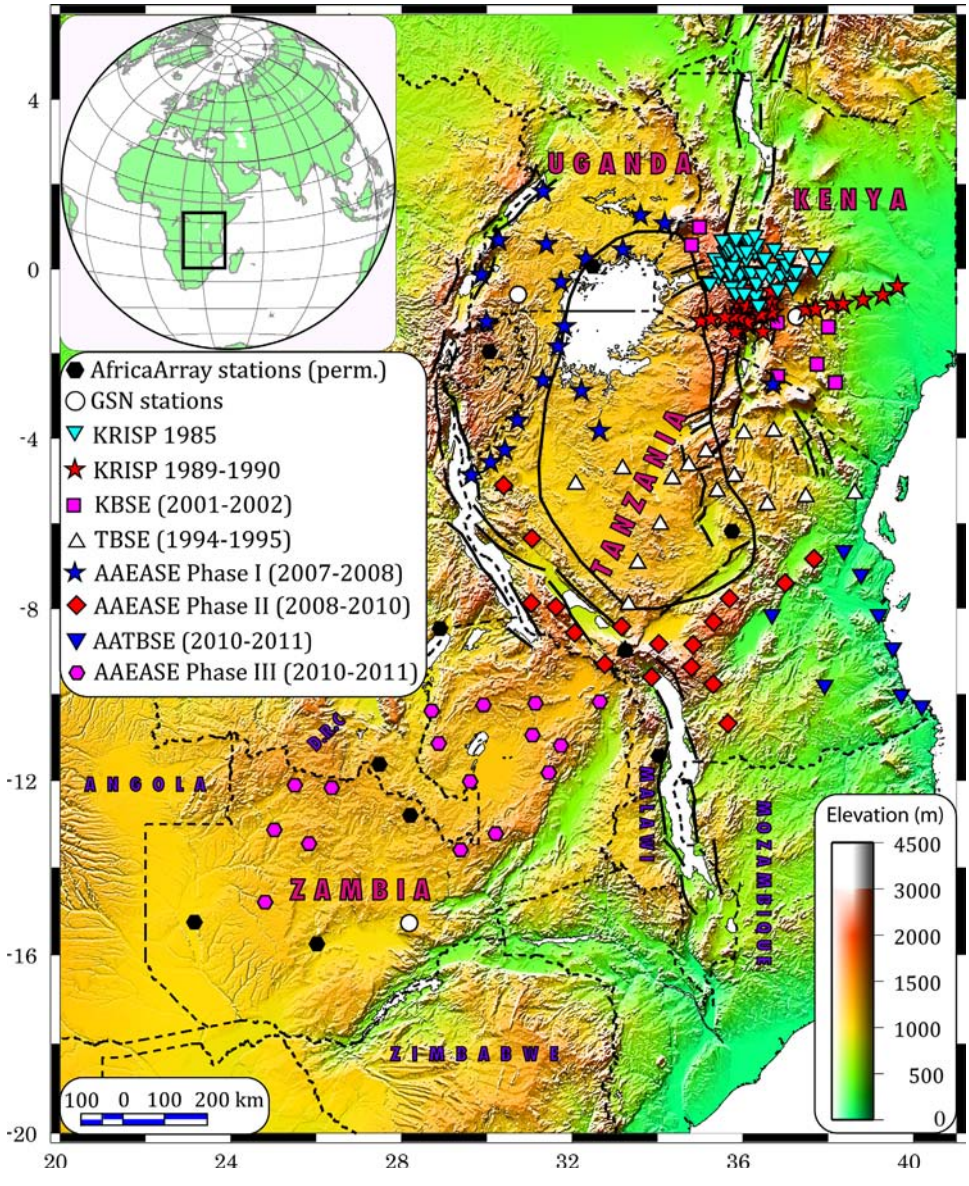


Figure 2. Topographic map showing seismic station locations used for this study. The dashed lines define the political boundaries and the bold lines show the outline of Tanzania Craton and the major rift faults. [Color figure can be viewed in the online issue, which is available at wileyonlinelibrary.com.]

volcanism in the Western branch commenced at ca. 25 Ma in the Rungwe Province [*Roberts et al*., 2012], at ca. 12 Ma in the Virunga Province, and at ca. 8 Ma in the Kivu Province [e.g., *Ebinger et al*., 1989; *Kampunzu et al*., 1998].

[9] The region is also characterized by a broad plateau, with a mean elevation of ~1000 m (Figure 2). The timing of plateau uplift is uncertain. A recent study by *Roberts et al*. [2012] found that plateau uplift may have begun as early as ca. 25 Ma, but there is also evidence of Neogene uplift along the flanks of some rift valleys in the eastern part of the plateau [e.g., *Noble et al*., 1997; *Spiegel et al*., 2007].

2.2. Previous Seismic Studies

[10] Studies using data from previous seismic deployments in Kenya and Tanzania have demonstrated the presence of a LWA in the upper mantle beneath the Eastern branch extending to depths of at least 400–500 km. Using *P* and *S* wave travel time tomography, *Ritsema et al*. [1998] imaged a LWA in the upper mantle beneath the Eastern branch dipping to the west under the Tanzania Craton and extending to ≥400 km depth. *Ritsema et al*. [1998] also imaged a region of fast wave speeds beneath the Tanzania Craton, showing that the lithospheric keel of the craton extends to a depth of ~150–200 km. The

westward dipping LWA was attributed to the flow of a mantle plume around the lithospheric keel of the Tanzania Craton by *Nyblade et al*. [2000].

[11] A P wave tomography study of the mantle beneath Kenya by *Park and Nyblade* [2006] also revealed the presence of a LWA dipping to the west beneath the Tanzania Craton, consistent with earlier tomographic models from the Kenya Rift International Seismic Project (KRISP) [*Green et al*., 1991; *Achauer and the KRISP Teleseismic Working Group*, 1994; *Achauer and Masson*, 2002]. The limited resolution imposed by the small aperture of the Tanzania and Kenya networks, however, made it difficult for these studies to show conclusively whether the westward dipping LWA continued at depth beneath the Tanzania Craton connecting to a similar LWA under the Western branch, and also if the LWA extended through the transition zone.

[12] A study of mantle transition zone discontinuities by *Owens et al*. [2000] using receiver function stacks and the tomography model from *Ritsema et al*. [1998] found evidence for a 30–40 km depression of the 410 km discontinuity, a result that was latter corroborated by *Huerta et al*. [2009] using a larger data set from stations in Tanzania and Kenya. A depressed 410 km discontinuity confirms that the upper mantle LWA is largely a thermal structure and that it extends to depths $\geq$410 km. The 660 km discontinuity was not well imaged by these studies, leaving the depth extent of the anomalous structure uncertain.

[13] Using surface wave tomography, *Weeraratne et al*. [2003] showed that the LWA imaged beneath the Eastern branch extends beneath the lithospheric keel of the Tanzania Craton. A more recent surface wave tomography model from *Adams et al*. [2012] confirms this finding and shows that the LWA under the Tanzania Craton also extends into the transition zone and beneath the Western branch. Continental-scale surface wave studies show generally similar results to the regional studies [e.g., *Sebai et al*., 2006; *Pasyanos and Nyblade*, 2007; *Priestley et al*., 2008; *Fishwick*, 2010].

3. Data and Methodology

3.1. Data sets

[14] Both new and previously acquired data have been used in this study. New data come from 60 stations of the AfricaArray eastern Africa broadband seismic experiment (AAEASE) deployed in three phases between 2007 and 2011 in Uganda, Tanzania, and Zambia (Figure 2). The stations consisted of broadband seismometers (Streckeisen STS-2, Guralp 3T, ESP and 40T), 24-bit RefTek data loggers and GPS clocks. The spacing between the stations was on average between 100 and 200 km, and data were recorded continuously at 40 samples per second. The first phase was comprised of 20 stations deployed in Uganda and northwestern Tanzania (August 2007 to December 2008). Eighteen of the stations were removed and redeployed in southern Tanzania from January 2009 to July 2010 (Phase II), and between February 2010 and July 2011 eight additional broadband stations of the AfricaArray Tanzania basin seismic experiment (AATBSE) were installed in southeastern Tanzania. The last phase of the deployment was from August 2010 to July 2011, when stations in southern Tanzania were demobilized and installed in Zambia. Other data come from the Tanzania broadband seismic experiment (TBSE) [*Nyblade et al*., 1996], the Kenya broadband seismic experiment (KBSE) [*Nyblade and Langston*, 2002], the KRISP network [*Achauer and the KRISP Teleseismic Working Group*, 1994], and permanent AfricaArray (www.africaarray.org) and Global Seismographic Network (GSN) stations. Seismograms from earthquakes with $m_b \geq 5.0$, spanning a distance between 30° and 90° from each station for *P* waves and 30° and 84° for *S* waves, were used for this study (Figure 3; see *Mulibo* [2012] for event list).

[15] The combined *P* wave data set consists of 21,867 arrival times from 1770 earthquakes recorded by the broadband stations and 2000 arrival times from 195 earthquakes recorded by the KRISP stations, for a total of 23,867 arrival times from 1865 earthquakes. The combined *S* wave data set is comprised of 14,000 arrival times from 1196 events recorded by the broadband stations. The majority of the events are located between back azimuths of 30° and 110°, but the overall azimuthal coverage is good for both *P* and *S* wave data sets (Figure 3).

3.2. Relative Arrival Time Determination

[16] Both broadband and short period waveforms were filtered using a two-pole Butterworth filter with corner frequencies of 0.5 and 2 Hz for *P* waves, which were picked on vertical component seismograms, and 0.04 and 0.1 Hz for *S* waves, which were picked on transverse component seismograms. The relative arrival times were obtained using the multichannel cross-correlation technique (MCCC) of *VanDecar and Crosson* [1990]. The

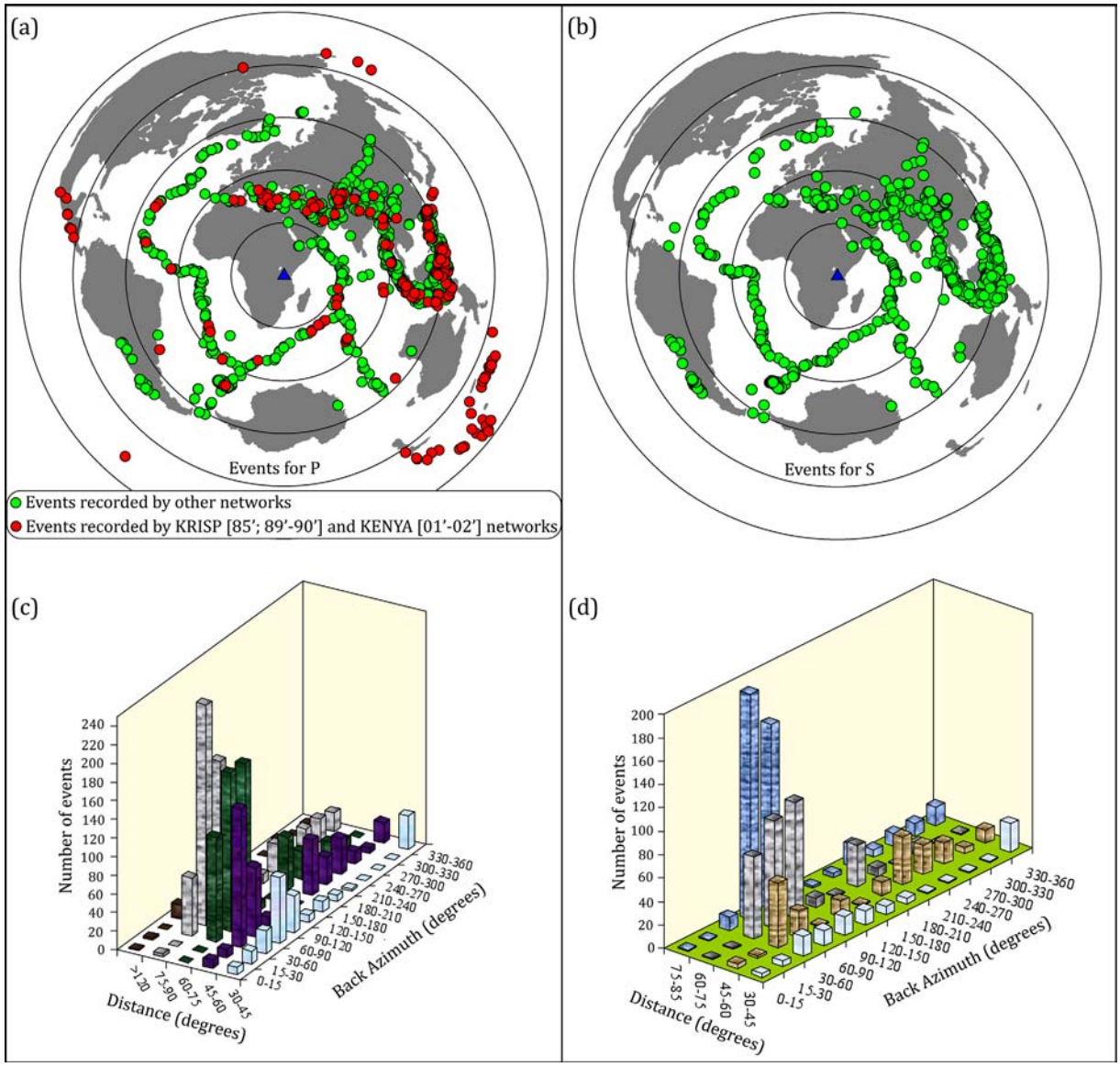


Figure 3. Event distribution of earthquakes used in this study for (a) *P* waves and (b) *S* waves. The blue triangle represents the center of the study region and the concentric circles represent great circles in 30° increments from the center of the study region. 3-D histograms for the distribution of the station-event pairs for (c) *P* waves and (d) *S* waves, with respect to epicentral distance and back azimuth. [Color figure can be viewed in the online issue, which is available at wileyonlinelibrary.com.]

method involves picking an arrival that is coherent on all waveforms for an event, finding a correlation maxima by cross correlating all possible waveform pairs, and applying a least squares optimization to obtain a relative arrival time for each station. Relative arrival time residuals for each station are then calculated using $t_i - (t_{ei} - t_{emean})$, where t_i is the relative arrival time for station i, t_{ei} is the expected IASP91 travel time [*Kennett and Engdahl*, 1991] for station i, and t_{emean} is the mean IASP91 travel time for the event.

[17] In this technique, the timing uncertainty of the relative arrival time residuals is estimated using the standard deviation for each station from the cross correlation function, which is on average 0.03 s for *P* waves and 0.1 s for *S* waves. The average variations in the relative arrival time residuals across the study region computed from the MCCC are 3 s and 4.5 s for *P* and *S* waves, respectively. The variations are comparable to the variations obtained in other similar studies in Tanzania [*Ritsema et al.*, 1998], Kenya [*Slack et al.*, 1994;

Park and Nyblade, 2006] and Ethiopia [*Bastow et al*., 2005, 2008; *Benoit et al*., 2006].

[18] Because the data were recorded during several different time periods, possible biases between the *P* and *S* wave arrival time data sets have been investigated by comparing arrival time delays for events recorded on collocated stations, computed by subtracting the observed arrival time from the theoretical travel time predicted by the IASP91 reference model [*Kennett and Engdahl*, 1991]. Arrival time delays computed for events from similar back azimuth and great circle distances do not show any consistent differences between the data sets (Figure 4; Supporting information, Figures S1a and S1b), and therefore we simply combined all of the relative arrival time residuals for the inversions.

3.3. Model Parameterization

[19] The model parameterization extends over more than 24° of latitude from 8°N to 23°S, over 28° of longitude from 18°E to 46°E, and from the surface to 1200 km depth. We parameterize the model space with splines under tension pinned at a series of regular knots [*Neele et al*., 1993]. The model consists of 32 knots in depth, 70 knots in latitude and 63 knots in longitude, amounting to a total of 141,120 knots (see Supporting information, Figure S3). The spacing of the knots in the inner most part of the model is 0.33° horizontally and 25 km vertically. The outer knots of the model are spaced 33 km apart between 200 and 700 km depth, 50 km between 700 and 1000 km depth, and 100 km between 1000 and 1200 km depth. The horizontal knot spacing increases from 0.5° to 1° moving from the inner most regions to the outermost region. The one–dimensional IASP91 radial earth model was used as a starting model for the inversion [*Kennett and Engdahl*, 1991].

3.4. Inversion of Arrival Time Residuals

[20] The relative arrival time residuals have been inverted for a three-dimensional (3-D) velocity model using *VanDecar*'s [1991] method. The method makes use of the infinite-frequency approximation by assuming that the energy travels from the source to the receiver solely along a ray path [*VanDecar et al*., 1995], an approximation that is useful when imaging structure with wavelengths greater than the wavelengths of the seismic waves. The method simultaneously inverts for slowness perturbations, station terms, and event relocations using an iterative procedure (conjugate gradients). Regularization by damping was not used to avoid biasing the solution toward the IASP91 model, which may not necessarily represent a good background model for the study area [*Mercier et al*., 2009]. The inversion includes station terms to absorb anomalies associated with the region directly beneath the stations where a lack of crossing rays prevents the resolution of crustal and uppermost mantle structure. Event relocations account for the effects of heterogeneous structure outside the model domain. Optimum smoothing and flattening parameters were selected through exploring trade-off curves as a subjective compromise between fitting the data and model roughness, with attention given to the estimated uncertainties in the data (Supporting information, Figure S4). The final *P* wave model, obtained using a smoothing of 100,000 and a flattening of 4000, explains 95% of the *P* wave RMS residual (from 0.782 s to 0.0039 s), and the final *S* wave model, obtained using a smoothing of 100,000 and a flattening of 4000, explains 97% of the *S* wave RMS residual (from 6.67 s to 0.226 s). The station terms are shown in Figures 5a and 8a.

4. Body Wave Tomographic Models

4.1. *P* wave Model

[21] Results for the *P* wave inversion are shown in Figure 5 and Figure S5 (Supporting information). Depth slices and cross sections through the model reveal regions of lower wave speeds of approximately $\delta Vp = \sim -1.0$ to -2.0% and regions of higher wave speeds of $\delta Vp = \sim 0.6$ to 1.0%. Model slices shallower than 100 km depth are not shown because of insufficient crossing ray coverage to clearly resolve structure there.

[22] Depth slices at 100 and 200 km depth (Figures 5a and 5b) show a LWA of $\delta Vp = \sim -1.0$ to -1.5% well developed beneath the two branches of the East African rift system and $\delta Vp = \sim -0.5\%$ beneath northwestern Zambia. The LWA beneath the Eastern branch mostly mimics the trend of the rift structures that impinge and penetrate to some extent into the Tanzania Craton. In the Western branch, the LWA is more pronounced in areas with volcanics (e.g., Virunga, Kivu and Rungwe provinces). A fast wave speed anomaly of $\delta Vp = \sim 0.6$ to 1.0% is observed at depths down to 300–350 km beneath the central and northern parts of the East African Plateau comprised of the Tanzania Craton and the Uganda Basement Complex,

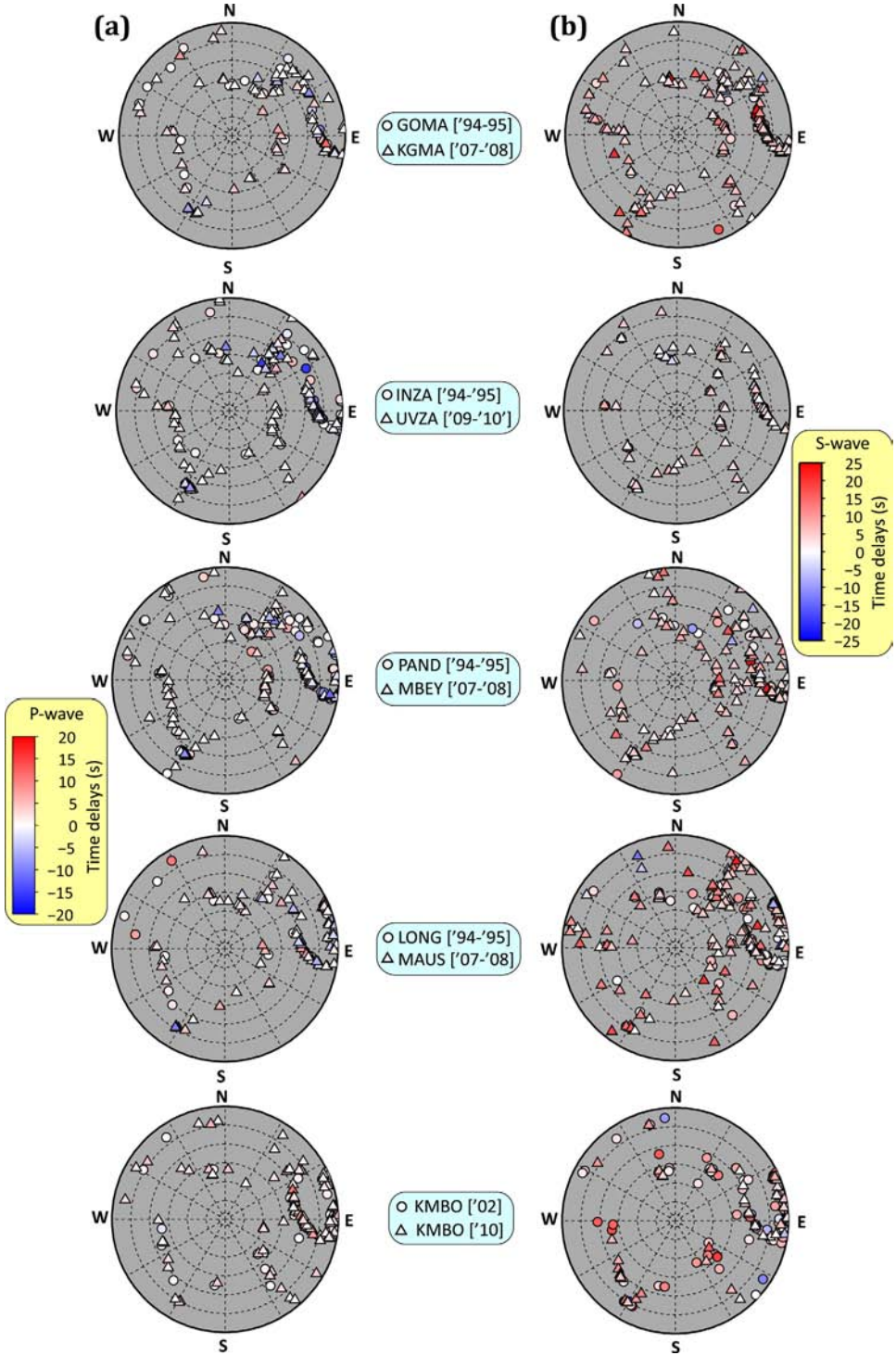


Figure 4. Polar plots showing variation of arrival time delays for (a) *P* waves and (b) *S* waves for events recorded on collocated stations between various networks. The concentric circles represent great circles in 15° increments from the stations. *P* wave arrival time delays for events recorded on collocated stations between the Kenya broadband seismic experiment (2001–2002) and the KRISP networks (1985 and 1989–1990) are shown in *Park and Nyblade* [2006]. [Color figure can be viewed in the online issue, which is available at wileyonlinelibrary.com.]

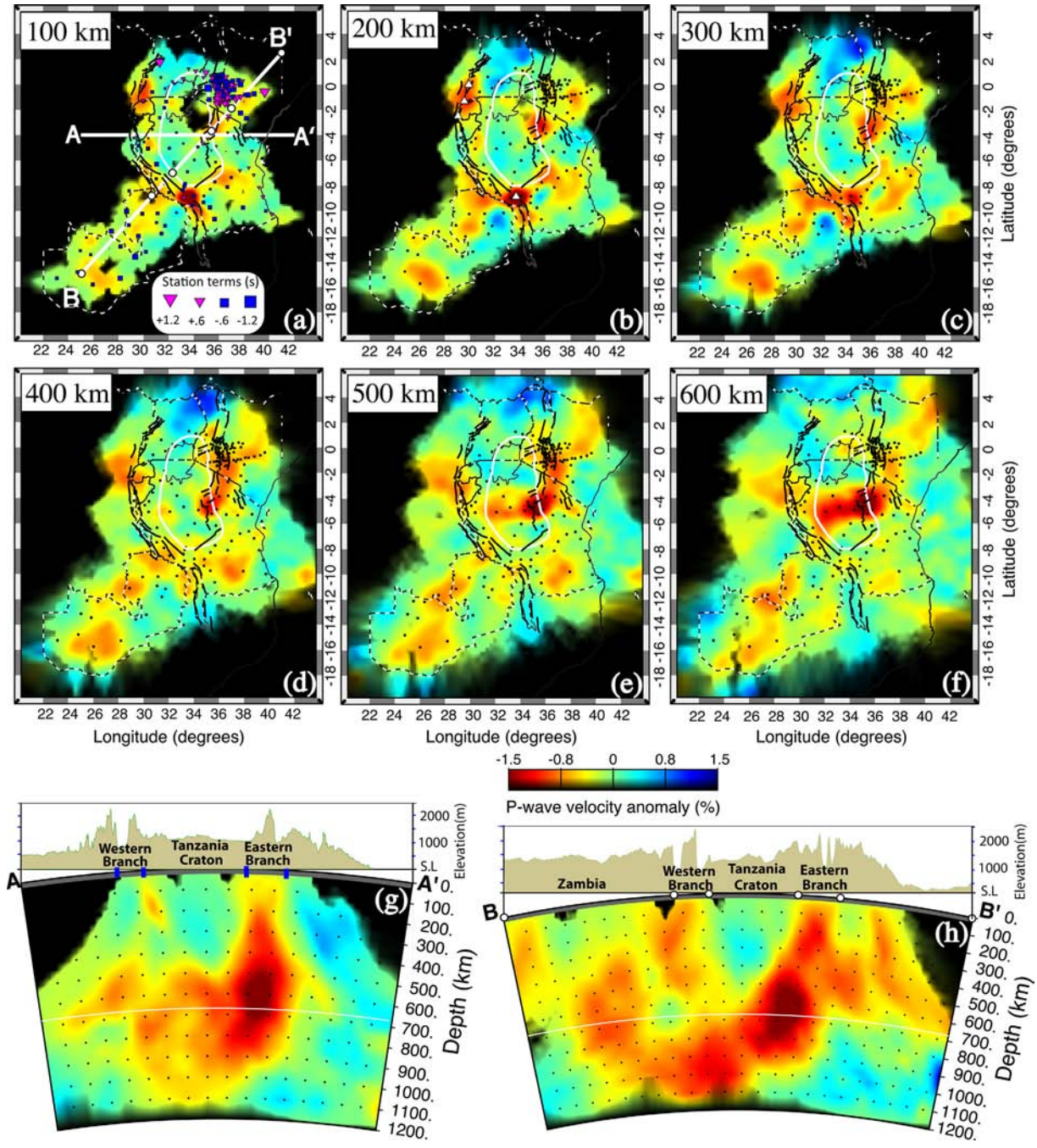


Figure 5. (a–f) Horizontal cross sections through the *P* wave velocity model at 100 km intervals from 100 to 600 km depth. Inverted pink triangles and blue squares show the station terms. (g and h) Vertical slices for profiles A–A' and B–B', whose locations are given in Figure 5a. Areas with hit counts of <5 are darkened. Small black squares represent station locations, Cenozoic rift faults are shown with bold black lines and the locations of volcanic centers along the Western branch are shown with white triangles in Figure 5b. The dashed lines define the political boundaries, and the bold white line shows the outline of the Tanzania Craton. [Color figure can be viewed in the online issue, which is available at wileyonlinelibrary.com.]

and beneath the eastern and central parts of Zambia comprised of the Irumide Belt. A region of fast wave speeds ($\delta Vp \geq 1\%$) is seen along the very northern edge of the model at depths ≥ 300 km.

[23] At deeper depths (>350 km), the LWA is most prominent under the central and southern parts of the East African Plateau and extends into the transition zone (Figures 5c and 5d). At

transition zone depths and within the upper part of the lower mantle (Figures 5e and 5f, and Supporting information, Figure S5) the LWA shifts to the southwest beneath northern Zambia. The anomaly is continuous across the transition zone and into the lower mantle. Figures 5g and 5h show depth slices through the model that cross the study region from E to W and diagonally from SW to NE. These figures show the LWA extending from depths of ~100 km to at least 900 km. The LWA has a maximum amplitude of −2% within and just below the transition zone.

4.2. *P* wave Resolution Tests

[24] To evaluate the resolution of the models, which depend mainly on the crossing ray paths within the model space, checkerboard and "tabular body" resolution tests have been performed. The checkerboard test were comprised of an alternating pattern of positive and negative (±5%) spherical velocity anomalies with diameter of 100 km inserted in one depth layer at a time for depths of 200, 300, 500, and 700 km. Synthetic arrival time data for the input models were generated using the actual ray paths, and a random time error with a standard deviation of 0.03 s was added to them. The synthetic arrival times were subsequently inverted for seismic wave speed structure using identical model parameters as used to invert the real data set. Results for the checkerboard tests show good lateral resolution for the entire region, with the horizontal dimensions of the spheres being well resolved at all depths (Figures 6a–6h). In contrast, up to 100 km of vertical smearing of the input spheres both downward and upward is observed due to the subvertical raypaths of the teleseismic *P* waves (Figures 6e–6h). All input bodies are resolved with an amplitude recovery of ~50–60%.

[25] Several sets of synthetic anomalies using tabular bodies were explored to investigate further the extent of vertical smearing and the structure of the LWA in the tomographic models (Figures 5g, 5h, 8g, and 8h). A test was done using two tabular bodies, one placed on top in the upper mantle and transition zone with fixed dimensions, representing the upper mantle LWA beneath eastern Africa, and a second body placed in the lower mantle with its top below the transition zone, representing the lower mantle LWA of the African superplume. The input anomaly for the body on top extends from the surface to 650 km depth with an amplitude of −5% (Figures 7a–7c), consistent with the previous studies of the transition zone discontinuities showing that the LWA extends to >410 km depth [*Owens et al*., 2000; *Huerta et al*., 2009]. The top surface of the second body was placed at depths of 750 and 850 km (Figures 7a and 7b), creating a separation between the two bodies of 100 and 200 km across and just below the bottom of the transition zone. An additional test was done using just the structure above 660 km depth (Figure 7c). Similar to the checkerboard tests, a synthetic arrival time data set was generated for each model and then inverted.

[26] The recovered images obtained from the inversion are shown in Figures 7d–7f and can be used to evaluate the possible connectivity of the two bodies. All input bodies are resolved with an amplitude recovery of ~50–60%. With a 100 km separation the bodies smear together (Figure 7d). At a separation of 200 km (Figure 7e), while there is still some connectivity of the two structures, the image shows two fairly distinct bodies. The models in Figures 7c and 7f show that the upper body smears downward by about 100 km, consistent with the checkerboard results.

[27] Given the amount of vertical smearing (i.e., ~100 km both upward and downward), it is possible that there could be a ~200 km separation between the upper and lower mantle structures that is not resolvable. However, the separation of the structures (i.e., the LWA of the African superplume in the lower mantle and the LWA in the upper mantle beneath eastern Africa) can be no greater than ~200 km. Consequently, if the LWA beneath eastern Africa extends well into the transition zone, as indicated by the depression of the 410 km discontinuity [*Owens et al*., 2000; *Huerta et al*., 2009] and regional body and surface wave tomography models [*Ritsema et al*., 1998; *Adams et al*., 2012], then the top of the lower mantle LWA must either extend upward to the 660 km discontinuity or to within 100–200 km of it.

4.3. S wave Model

[28] The *S* wave model is similar to the *P* wave model (Figures 8a–8h and Supporting information, Figure S5). The LWA at depths between 100 and 200 km beneath the Eastern and Western branches has amplitudes of ~−1 to −2%, and ~−0.5% beneath northwestern Zambia. A fast wave speed anomaly of $\delta Vs = \sim 0.8$ to 1% is seen at depths down to 300–350 km under the central and northern parts of the East African Plateau and beneath

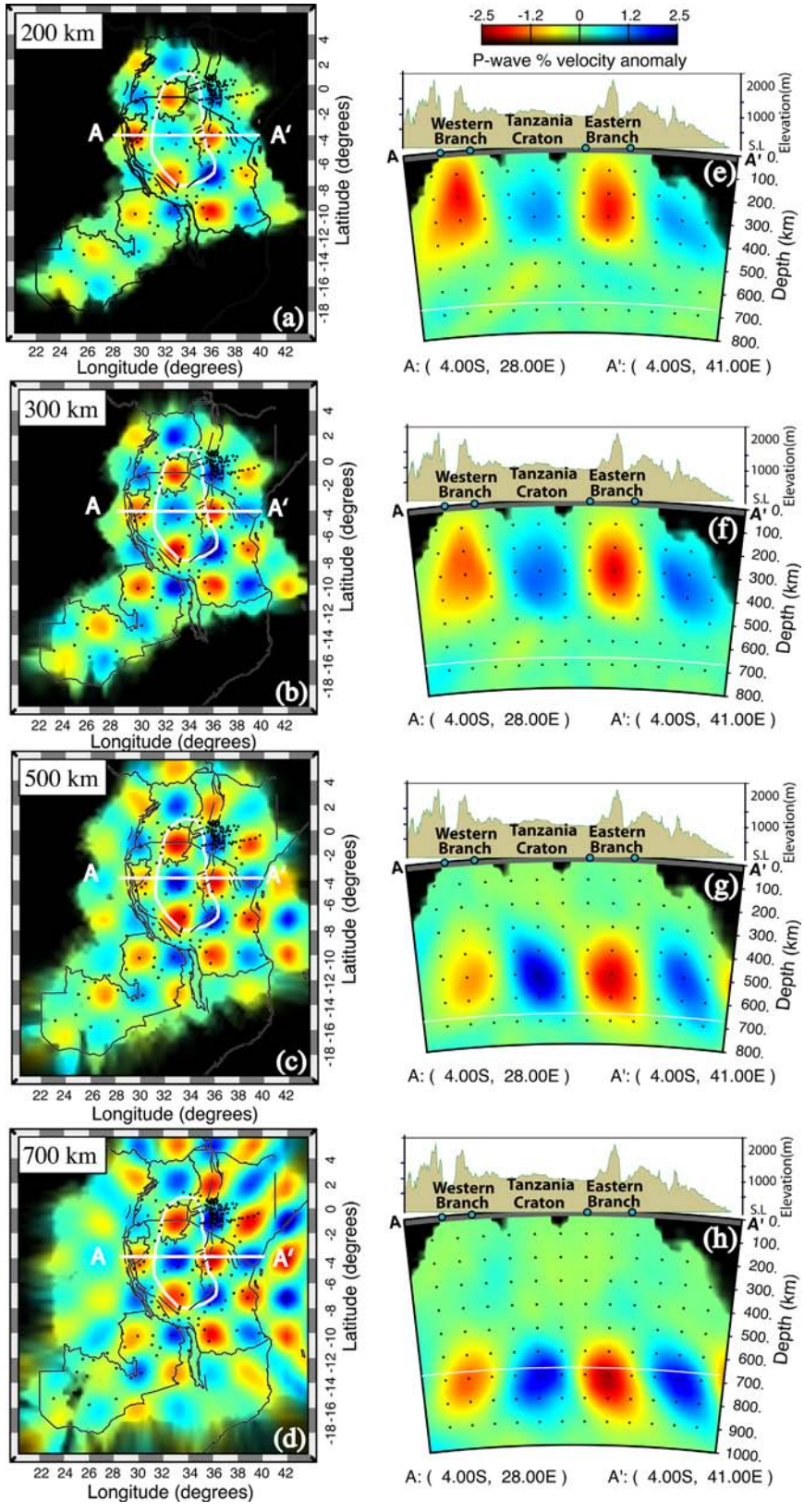


Figure 6. Depth slices and cross sections showing checkerboard resolution test results for the *P* wave model. Recovered models are from an input model of alternative 100 km diameter Gaussian spheres with ±5% peak velocity anomaly at depths of 200, 300, 500, and 700 km. Areas with hit counts of <5 are darkened. Small black squares represent station locations and Cenozoic rift faults are shown with bold black lines. The dashed lines define the political boundaries, and the bold white line shows the outline of the Tanzania Craton. [Color figure can be viewed in the online issue, which is available at wileyonlinelibrary.com.]

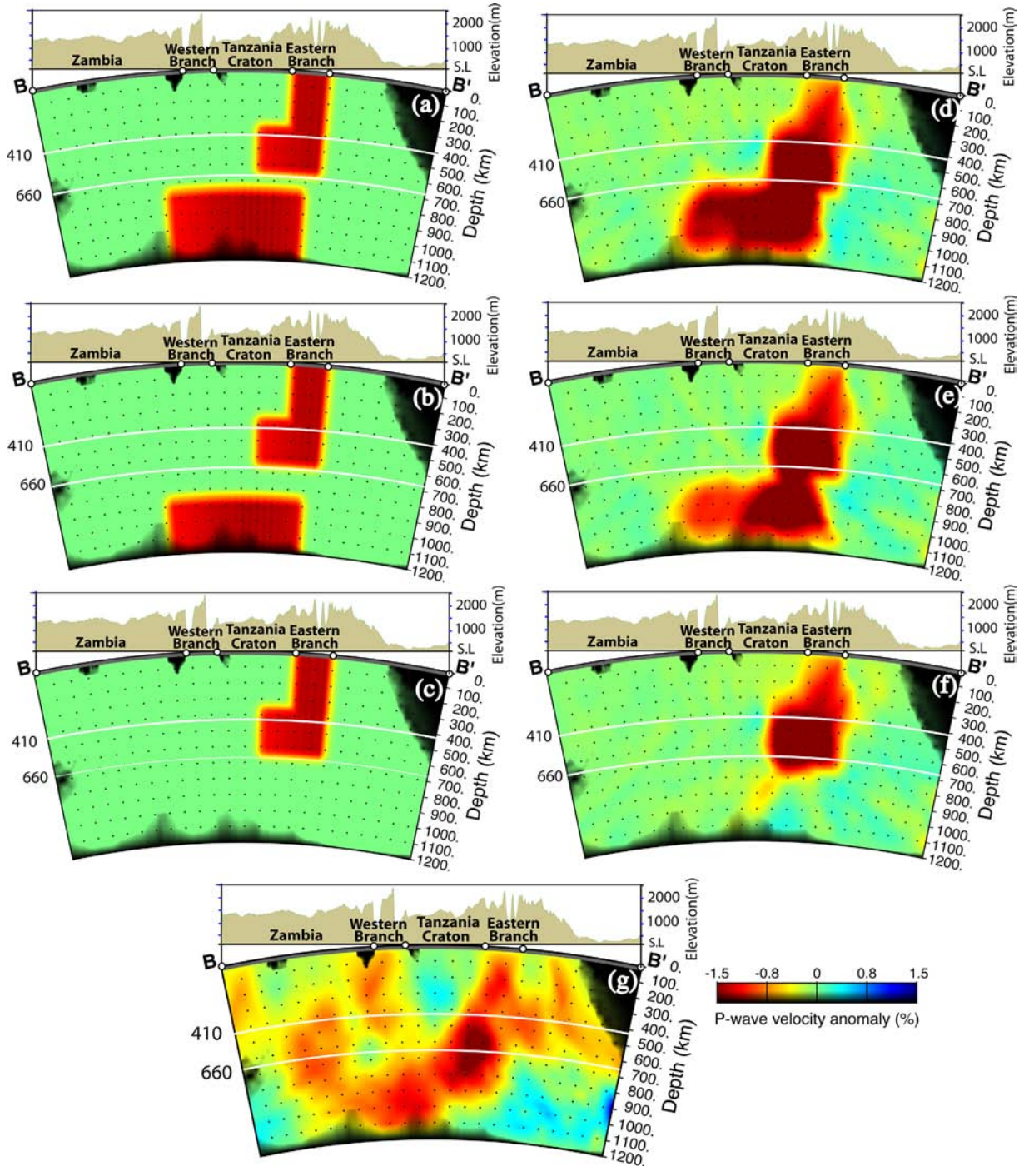


Figure 7. Tabular body test for the *P* wave model. (a–c) Input models and (d–f) recovered models. See text for further explanation. (g) Cross section along profile BB' shown in Figure 5a. Areas of the model with hit counts <5 are darkened. [Color figure can be viewed in the online issue, which is available at wileyonlinelibrary.com.]

the eastern and central parts of Zambia. And a region of faster wave speeds ($\delta Vs \geq 0.5\%$) is seen along the very northern edge of the model at depths ≥ 300 km.

[29] Also similar to the *P* wave model, the LWA at deeper depths is most prominent under the central and southern parts of the East African Plateau, and extends into and through the transition zone. The

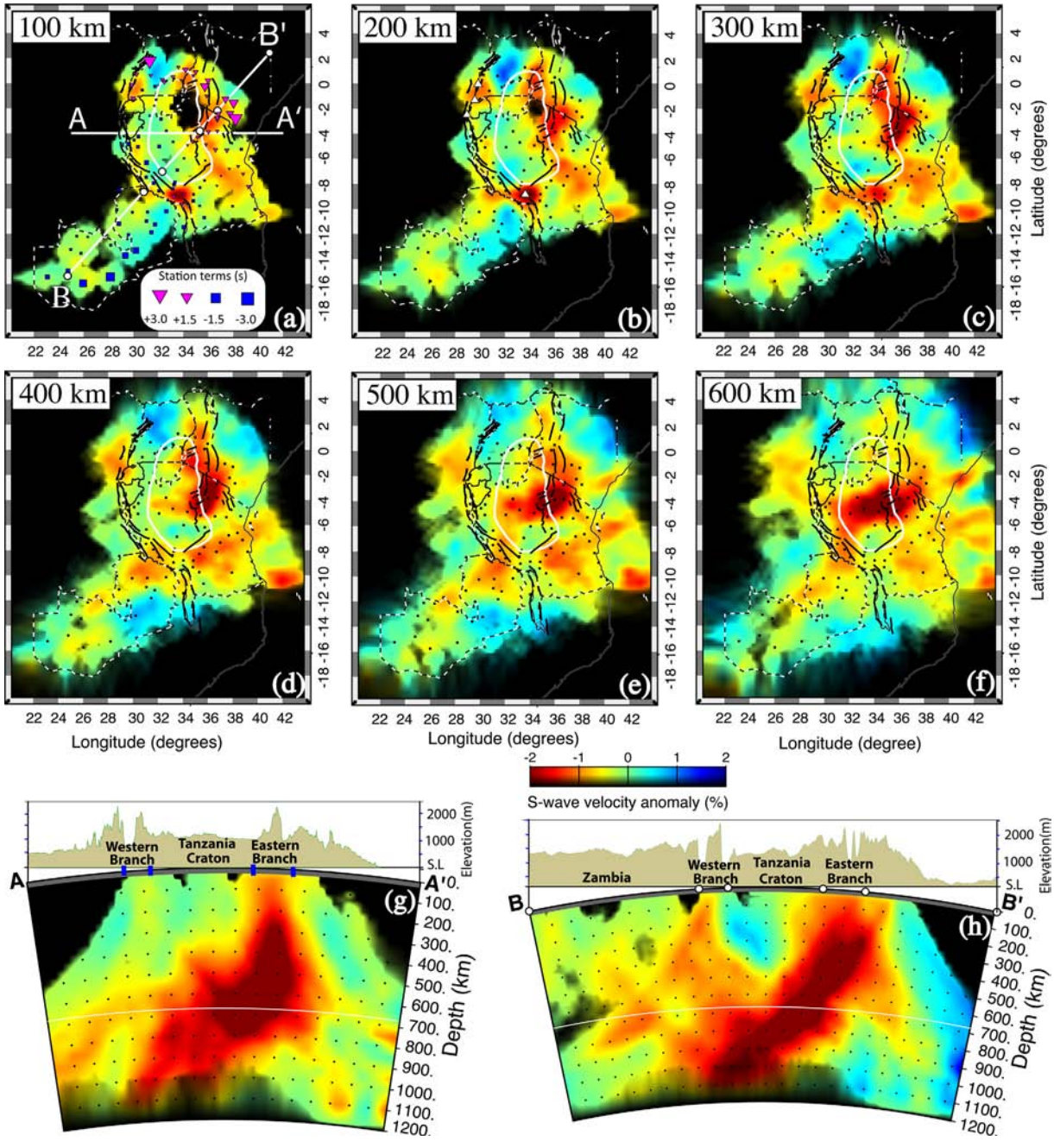


Figure 8. (a–f) Horizontal cross sections through the *S* wave velocity model at 100 km intervals from 100 to 600 km depth. Inverted pink triangles and blue squares show the station terms. (g and h) Vertical slices for profiles A–A' and B–B', whose locations are given in (a). Areas with hit counts of <5 are darkened. Small black squares represent station locations, Cenozoic rift faults are shown with bold black lines and the locations of volcanic centers along the Western branch are shown with white triangles in Figure 8b. The dashed lines define the political boundaries, and the bold white line shows the outline of the Tanzania Craton. [Color figure can be viewed in the online issue, which is available at wileyonlinelibrary.com.]

anomaly shifts to the southwest beneath northern Zambia at transition zone depths and within the top part of the lower mantle, as seen in the *P* wave model, illustrating the continuity of the anomaly across the transition zone and into the lower mantle. Cross sections through the model (Figures 8g and 8h) show the same structural features as described previously in the *P* wave model (Figures 5g and

5h). The LWA has a maximum amplitude of −3% within and just below the transition zone.

4.4. *S* wave Resolution Tests

[30] Checkerboard and "tabular body" tests similar to the *P* wave resolution tests have been performed using the *S* wave data set. The same input models were used as for the *P* wave resolution tests, but a random error of 0.1 s was added to the synthetic relative arrival time residuals. Results for the *S* wave checkerboard test are illustrated in Figures 9a–9h, which show similar resolution to the *P* wave model for 100 km radius spheres at 200, 300, 500, and 700 km depths. The *S* wave "tabular body" test shows smearing together of the two bodies when a separation of 100 km is used (Figure 10d), but for a separation of 200 km, the image shows two fairly distinct bodies (Figure 10e), similar to the results obtained for the *P* wave model.

5. Discussion

[31] In summary, the main features of the *P* and *S* wave models are a LWA at shallow depths (100–200 km) beneath many parts of the Eastern and Western branches of the rift system and northwestern Zambia, and a fast wave speed anomaly at depths above ∼300–350 km beneath the central and northern parts of the East African Plateau and the eastern and central parts of Zambia. At deeper depths (≥350 km), the LWA in both the *P* and *S* wave models coalesces under the central and southern parts of the East African Plateau and extends into the transition zone. Below the transition zone, the LWA dips to the southwest beneath northern Zambia, extending to a depth of at least 900 km. Resolution is similar for both the *P* and *S* models and indicates that there can be at most only 200 km of separation between an upper and a lower mantle anomaly in order to explain a LWA that extends through the transition zone into the lower mantle, as seen in Figures 5 and 8.

[32] At shallow mantle depths, the LWA beneath northwestern Zambia may represent a secondary Western rift branch extending southwestward from Lake Tanganyika, as suggested by *O'Donnell et al*. [2013], and the fast wave speed anomaly imaged beneath the eastern and central parts of Zambia may represent a southeastward extension of the Bagweulu Block [*O'Donnell et al*., 2013]. To the north, the fast wave speed anomaly observed beneath the Uganda Basement Complex is likely thick Archean lithosphere [*Begg et al*., 2009; *Adams et al*., 2012]. The fast wave speed anomaly along the very northern edge of the *P* and *S* wave models extending to depths > 300 km is probably not well resolved and may be caused by vertical smearing of fast upper most mantle beneath the Uganda Basement Complex.

[33] Mantle velocities can be strongly influenced by temperature variations and to a lesser extent by compositional variations, partial melt, water, and anisotropy [e.g., *Sobolev et al*., 1996; *Goes et al*., 2000; *Griffin et al*., 2003]. For eastern Africa, water content is not considered to be an important factor because there has not been any subduction in this region for ≥500 Ma. The presence of Cenozoic volcanism in some places clearly suggests that partial melts may locally influence mantle velocities, and compositional differences between Archean and younger lithosphere could also contribute to mantle wave speed variations. The pattern of anisotropy is complex, and it is less obvious how this might affect mantle velocities [*Bagley and Nyblade*, 2013; *Walker et al*., 2004].

[34] The temperature perturbation indicated by the amplitude of the LWA can be estimated by using a shear wave temperature derivative of 8×10^{-4} km/s/K, obtained for a grain size of 10 mm at an average upper mantle temperature of 1300°C [*Faul and Jackson*, 2005; *Wiens et al*., 2008]. Using the maximum *S* wave velocity anomaly of $\delta Vs = \sim -3.0\%$, a temperature anomaly of ∼300 K is obtained, while the mean and median values of $\delta Vs = \sim -2.0\%$ and $\delta Vs = \sim -1.5\%$ yield a thermal anomaly of ∼200 K and ∼150 K, respectively. These perturbations are consistent with the temperature anomaly of 200–350 K estimated at the top of the transition zone from receiver function stacks [*Owens et al*., 2000; *Huerta et al*., 2009] and 280 K from seismic attenuation in the upper mantle [*Venkataraman et al*., 2004]. Although the amplitude of the LWA in the mantle imaged in this study can be attributed entirely to elevated temperatures, it is also possible, as mentioned above, that partial melt, compositional variations, and anisotropy may contribute to the anomaly, although probably to a lesser extent than temperature.

[35] The depth extent of the LWA revealed in our model (Figures 5g, 5h, 8g, and 8h) indicates that the superplume structure in the lower mantle connects to anomalous structure in the upper mantle beneath eastern Africa to form a through-going mantle anomaly. As illustrated by our resolution tests, the LWA associated with the superplume

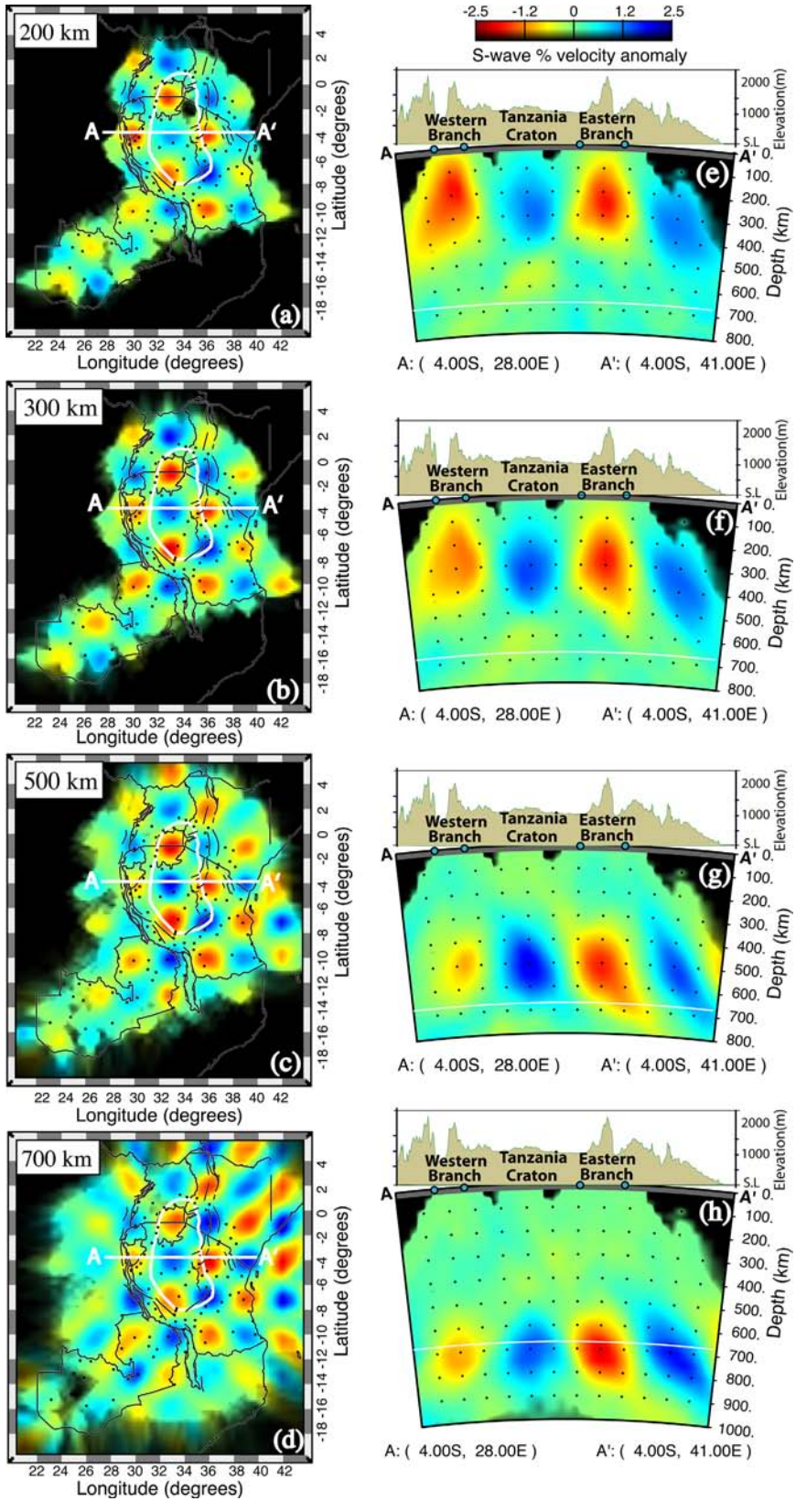


Figure 9. Depth slices and cross sections showing checkerboard resolution test results for the *S* wave model. Recovered models are from an input model of alternative 100 km-diameter Gaussian spheres with ±5% peak velocity anomaly at depths of 200, 300, 500, and 700 km. Areas with hit counts of <5 are darkened. Small black squares represent station locations and Cenozoic rift faults are shown with bold black lines. The dashed lines define the political boundaries and the bold white line shows the outline of the Tanzania Craton. [Color figure can be viewed in the online issue, which is available at wileyonlinelibrary.com.]

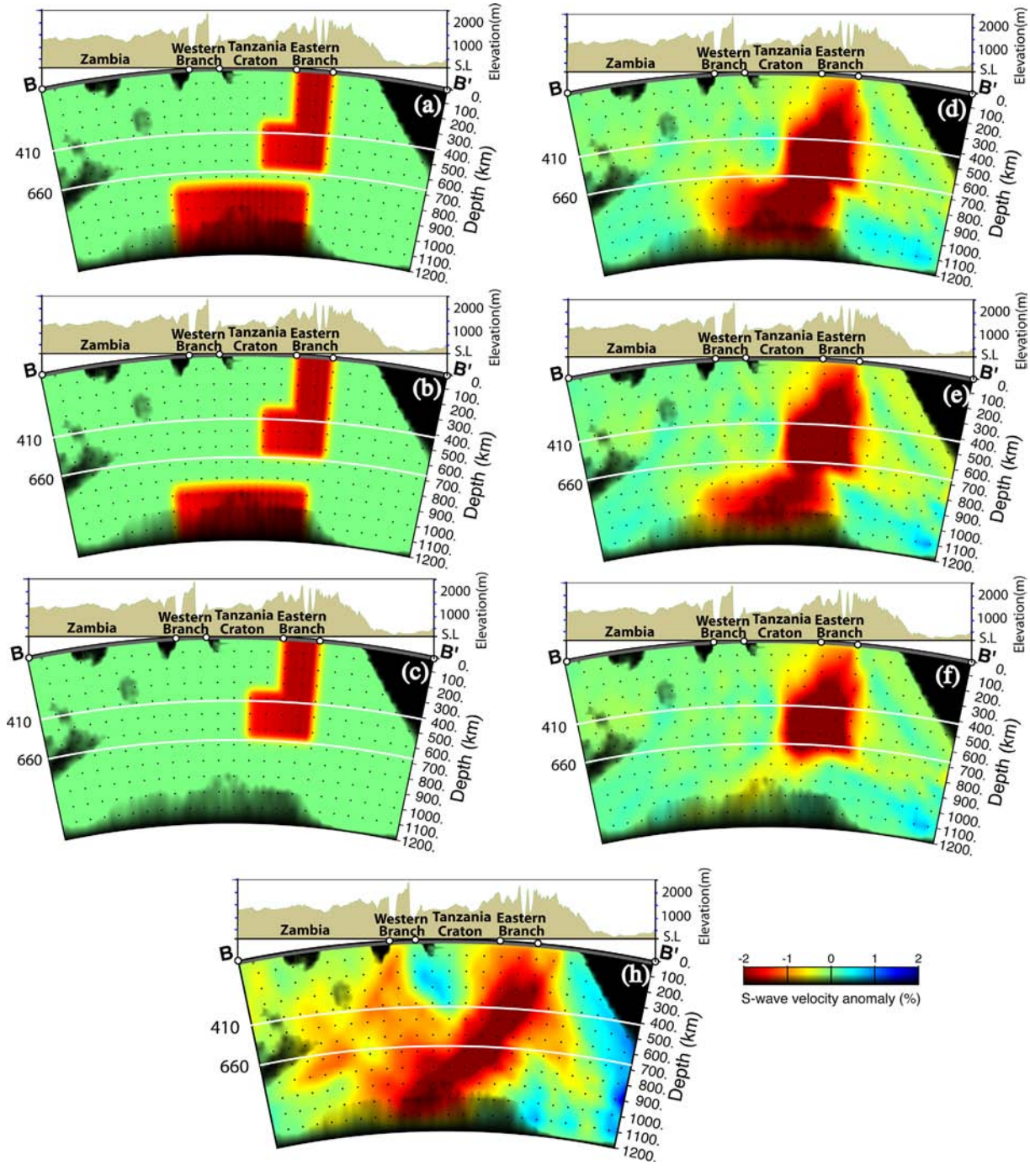


Figure 10. Tabular body test for the *S* wave model. (a–c) Input models and (d–f) recovered models. See text for further explanation. (g) Cross section along profile BB' shown in Figure 5a. Areas of the model with hit counts <5 are darkened. [Color figure can be viewed in the online issue, which is available at wileyonlinelibrary.com.]

must either extend upward to the 660 km discontinuity or else to within 100 or 200 km of the discontinuity. If the upper and lower mantle anomalies are primarily thermal in origin as indicated by *Owens et al*. [2000], *Huerta et al*. [2009] and *Davies et al*. [2012], and long-lived [*Hager*, 1985; *Forte and Mitrovica*, 2001; *Forte et al*., 2002], then in all probability there is at least a thermal connection between them. Even if the top of the superplume structure is 100–200 km below the 660 km discontinuity, it would still lead to heating of the transition zone over many 10s of millions of years, forming a

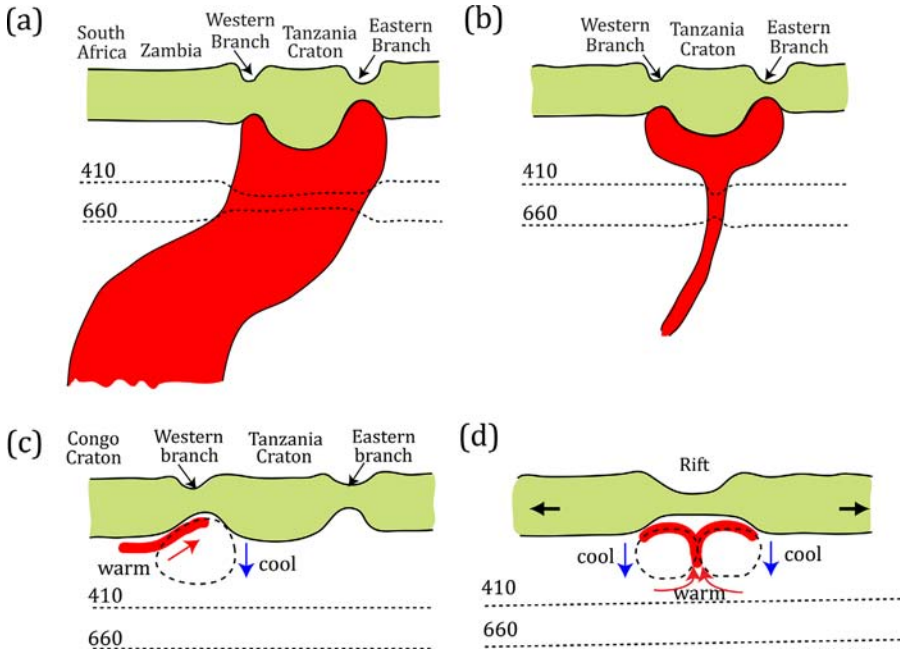


Figure 11. Geodynamic models proposed for the origin of the Cenozoic rifting, volcanism and plateau uplift in eastern Africa; (a) superplume model, (b) single plume model, (c) edge flow convection, and (d) small-scale convection induced by passive stretching of the lithosphere. [Color figure can be viewed in the online issue, which is available at wileyonlinelibrary.com.]

continuous thermal structure extending from the core-mantle boundary to the surface. Some of the superplume structure might also be compositionally anomalous [*Simmons et al*., 2007], and there could be material flowing from the lower to the upper mantle, as suggested by geochemical evidence [e.g., *Hilton et al*., 2011; *Pik et al*., 2006], which we cannot detect.

[36] Given this conclusion, a superplume origin for the Cenozoic tectonism in eastern Africa is favored. If lower mantle material flows across the transition zone, then this material would continue to rise through the upper mantle and provide the excess heat needed to drive the rifting and plateau uplift (Figure 11a). Alternatively, if the superplume simply heats the base of the transition zone, then several smaller plumes above the 660 km discontinuity could form, rise through the upper mantle, and lead to extension and surface uplift [e.g., *Yuen et al*., 2007; *Maruyama et al*., 2007].

[37] As reviewed previously, many single plume models have been invoked to explain the Cenozoic rifting, volcanism and plateau uplift in eastern Africa. A single large plume (Figure 11b) would not produce a wide enough anomaly to account for the LWA in the transition zone (Figures 5g, 5h, 8g, and 8h). Other models that have been proposed to explain the Cenozoic tectonism include edge-flow convection (Figure 11c) and passive stretching of the lithosphere (Figure 11d). Edge-driven convection (Figure 11c) leads to small-scale thermal upwellings confined to depths of less than ~350 km, inconsistent with the tomographic models in Figures 5g, 5h, 8g, and 8h. The LWA in the transition zone is several hundreds of kilometers wide, and such a wide and deep thermal structure is difficult to explain with edge flow around the sides of cratonic lithosphere. Passive stretching of the lithosphere (Figure 11d) results in small-scale convection beneath thinned lithosphere, but similar to the edge-flow model, the thermal upwelling would not extend as deep as the transition zone, which is inconsistent with the depth extent of the LWA in Figures 5g, 5h, 8g, and 8h. The depth to which the small-scale convection cell can extend is limited by the <10% extension across the Cenozoic rifts [*Ebinger et al*., 1997; *Foster et al*., 1997].

6. Summary and Conclusions

[38] Mantle structure beneath eastern Africa has been investigated using body wave tomography, which reveals a LWA beneath many parts of the Eastern and Western branches of the rift system and northwestern Zambia at shallow depths (100–200 km). The models also show a fast wave speed

anomaly at depths of ≤300–350 km beneath the central and northern parts of the East African Plateau and the eastern and central parts of Zambia. At deeper depths (≥350 km) the LWA coalesces under the central and southern parts of the East African Plateau and extends into the transition zone. Below the transition zone, the LWA dips to the southwest beneath northern Zambia, extending to a depth of at least 900 km. The amplitude of the LWA can be attributed to a temperature perturbation of 150–300 K, consistent with the magnitude of the upper mantle temperature anomaly argued for previously by many authors. Even though the amplitude of the LWA can be attributed entirely to elevated temperatures, contributions to the anomaly could also come from partial melt, anisotropy and compositional variations.

[39] Using the deeper structure in our model, the nature of the superplume and geodynamic models for the Cenozoic tectonism in eastern Africa have been re-examined. Resolution tests permit at most 200 km of separation between the LWA in the upper mantle beneath eastern Africa and the lower mantle structure of the African superplume. Such a small separation, if one exists at all, indicates that the superplume is likely a through-going mantle thermal anomaly. A continuous anomaly extending from the core-mantle boundary beneath southern Africa to the surface beneath eastern Africa implies an origin for the Cenozoic extension, uplift and volcanism in eastern Africa that is rooted in the dynamics of the lower mantle.

Acknowledgments

[40] We would like to thank IRIS-PASSCAL, the Tanzania Geological Survey, the University of Dar es Salaam, the Uganda Geological Survey, the Zambia Geological Survey, Penn State University and many individuals from those institutions for their assistance with fieldwork. We also thank Yongcheol Park for providing *P* wave arrival time residuals for the KRISP data set and Maximiliano Bezada and an anonymous reviewer for helpful comments. This study was funded by the National Science Foundation (Grant numbers OISE-0530062, EAR-0440032, EAR-0824781).

References

Achauer, U., and the KRISP Teleseismic Working Group (1994), New ideas on the Kenya Rift based on the inversion of the combined dataset of the 1985 and 1989/90 seismic tomography experiments, *Tectonophysics*, *236*, 305–329.

Achauer, U., and F. Masson (2002), Seismic tomography of continental rifts revisited: From relative to absolute heterogeneities, *Tectonophysics*, *358*, 17–37.

Adams, A., A. A. Nyblade, and D. Weeraratne (2012), Upper mantle shear wave velocity structure beneath the East African plateau: Evidence for a deep, plateau wide low velocity anomaly, *Geophys. J. Int.*, *189*(1), 123–932, doi:10.1111/j.1365246X.2012.05373.x.

Bagley, B., and A. A. Nyblade (2013), Seismic anisotropy in eastern Africa, mantle flow, and the African superplume, *Geophys. Res. Lett.*, *40*, doi:10.1002/grl.50315, in press.

Bastow, I., G. Stuart, J. Kendall, and C. Ebinger (2005), Upper-mantle seismic structure in a region of incipient continental breakup: Northern Ethiopian rift, *Geophys. J. Int.*, *162*, 479–493.

Bastow, I., A. A. Nyblade, G. Stuart, T. O. Rooney, and M. H. Benoit (2008), Upper mantle seismic structure beneath the Ethiopian hot spot: Rifting at the edge of the African low-velocity anomaly, *Geochem. Geophys. Geosyst.*, *9*, Q12022, doi:10.1029/2008GC002107.

Begg, G. C., et al. (2009), The lithospheric architecture of Africa: Seismic tomography, mantle petrology, and tectonic evolution, *Geosphere*, *5*(1), 23–50, doi:10.1130/GES00179.1.

Benoit, M., A. A. Nyblade, and J. VanDecar (2006), Upper mantle P-wave speed variations beneath Ethiopia and the origin of the Afar hotspot, *Geology*, *34*, 329–332.

Buck, W. (1986), Small-scale convection induced by passive rifting: The cause for uplift of rift shoulders, *Earth Planet. Sci. Lett.*, *77*, 362–372.

Burke, K. (1996), The African plate, *South Afr. J. Geol.*, *99*, 341–409.

Cahen, L., N. Snelling, J. Delhal, and J. Vail (1984), *The Geochronology and Evolution of Africa*, Oxford Univ. Press, New York.

Catuneanu, O., H. Wopfner, P. G. Eriksson, B. Cairncross, B. S. Rubidge, R. M. H. Smith, and P. J. Hancox (2005), The Karoo basins of south-central Africa, *J. Afr. Earth Sci.*, *43*, 211–253, doi:10.1016/j.jafrearsci.2005.07.007.

Chang, S.-J., and S. Van der Lee (2011), Mantle plumes and associated flow beneath Arabia and East Africa, *Earth Planet. Sci. Lett.*, *302*, 448–454, doi:10.1016/j.epsl.2010.12.050.

Davies, D. R., S. Goes, J. H. Davies, B. S. A. Schuberth, H.-P. Bunge, and J. Ritsema (2012), Reconciling dynamic and seismic models of Earth's lower mantle: The dominant role of thermal heterogeneity, *Earth Planet. Sci. Lett.*, *353-354*, 253–269.

Dawson, J. (1992), Neogene tectonics and volcanicity in the North Tanzania Sector of the Gregory Rift Valley: Contrasts with the Kenya sector, *Tectonophysics*, *204*, 81–92.

De Waele, B., S. Johnson, and S. Pisarevsky (2008), Palaeoproterozoic to Neoproterozoic growth and evolution of the eastern Congo Craton: Its role in the Rodinia puzzle, *Precambrian Res.*, *160*, 127–141.

Dziewonski, A. (1984), Mapping the lower mantle: Determination of lateral heterogeneity in P velocity up to degree and order 6, *J. Geophys. Res.*, *89*(B7), 5929–5952.

Dziewonski, A., and J. Woodhouse (1987), Global images of the Earths interior, *Science*, *236*, 37–48.

Ebinger, C. (1989), Tectonic development of the western branch of the East Africa rift system, *Bull. Seismol. Soc. Am.*, *101*, 885–903.

Ebinger, C., and N. Sleep (1998), Cenozoic magmatism throughout east Africa resulting from impact of a single plume, *Nature*, *395*, 788–791.

Ebinger, C., T. Bechtel, D. Forsyth, and C. Bowin (1989), Effective elastic plate thickness beneath the East African and the Afar plateau and dynamic compensation for the uplifts, *J. Geophys. Res.*, *94*, 2883–2901.

Ebinger, C., Y. Poudjom, E. Mbede, F. Foster, and J. Dawson (1997), Rifting Archean lithosphere: The Eyasi-Manyara-

Natron rifts, East Africa, *J. Geol. Soc. London*, *154*, 947–960.

Faul U., and I. Jackson (2005), The seismological signature of temperature and grain size variations in the upper mantle, *Earth Planet. Sci. Lett.*, *234*, 119–134.

Fishwick, S. (2010), Surface wave tomography: Imaging of the lithosphere-asthenosphere boundary beneath central and southern Africa, *Lithos*, *120*, 63–73.

Forte, A. M., and J. X. Mitrovica (2001), Deep-mantle high-viscosity flow and thermo-chemical structure inferred from seismic and geodynamic data, *Nature*, *410*, 1049–1056.

Forte, A. M., J. X. Mitrovica, and A. Espesset (2002), Geodynamic and seismic constraints on the thermochemical structure and dynamics of convection in the deep mantle, *Philos. Trans. R. Soc. London A*, *360*, 2521–2543.

Foster, A., C. Ebinger, E. Mbede, and D. Rex (1997), Tectonic development of the northern Tanzania sector of the East African rift system, *J. Geol. Soc. London*, *154*, 689–700.

Furman, T., J. Bryce, T. Rooney, G. Yirgu, and D. Ayalew (2006), Heads and tails: 30 million years of the Afar plume, in *The Structure and Evolution of the East African Rift System in the Afar Volcanic Province*, edited by G. Yirgu, C. J. Ebinger, and P. K. H. Maguire, *Geol. Soc. London Spec. Publ. 259*, 97–121.

George, R., N. Rogers, and S. Kelley (1998), Earliest magmatism in Ethiopia: Evidence for two mantle plumes in one flood basalt province, *Geology*, *26*, 923–926.

Goes, S., R. Govers, and P. Vacher (2000), Shallow mantle temperatures under Europe from P and S-wave tomography, *J. Geophys. Res.*, *105*(B5), 11,153–11,169.

Green, W., U. Achauer, and R. Meyer (1991), A 3-dimensional seismic image of the crust and upper mantle beneath the Kenya rift, *Nature*, *354*, 199–203.

Griffin, W., S. O'Reilly, L. Natapov, and C. Ryan (2003), The evolution of lithospheric mantle beneath the Kalahari Craton and its margins, *Lithos*, *71*, 19–41.

Hager, B. H., R. W. Clayton, M. A. Richards, R. P. Comer, and A. M. Dziewonski (1985), Lower mantle heterogeneity, dynamic topography and the geoid, *Nature*, *313*, 541–545.

Hansen, S., A. A. Nyblade, and M. Benoit (2012), Mantle structure beneath Africa and Arabia from adaptively parameterized P-wave tomography: Implications for the origin of Cenozoic Afro-Arabian tectonism, *Earth Planet. Sci. Lett.*, *319-320*, 23–34.

Hilton, D. R, S. A. Halldorsson, P. H. Barry, T. P. Fischer, J. M. de Moor, C. J. Ramirez, F. Mangasini, and P. Scarsim (2011), Helium isotopes at Rungwe Volcanic Province, Tanzania, and the origin of East African Plateaux, *Geophys. Res. Lett.*, *38*, L21304, doi:10.1029/2011gl 049589.

Huerta, A., A. A. Nyblade, and A. Reusch (2009), Mantle transition zone beneath Kenya and Tanzania: More evidence for deep-seated thermal upwelling in the mantle, *Geophys. J. Int.*, *177*, 1249–1255.

Kampunzu, A., M. Bonhmme, and M. Kanika (1998), Geochronology of volcanic rocks and evolution of the Cenozoic western branch of the East Africa Rift System, *J. Afr. Erath Sci.*, *26*(3), 441–461.

Kennett, B., and E. Engdahl (1991), Traveltimes for global earthquake location and phase identification, *Geophys. J. Int.*, *122*, 429–465.

King, S. (2007), Hotspots and edge-driven convection, *Geology*, *35*, 223–226.

King, S., and L. Anderson (1995), An alternative mechanism of flood basalt formation, *Earth Planet. Sci. Lett.*, *136*(3–4), 269–279.

King, S., and J. Ritsema (2000), African hot spot volcanism: Small-scale convection in the upper mantle beneath cratons, *Science*, *290*, 1137–1140.

Macdonald, R., N. Rogers, J. Fitton, S. Black, and M. Smith (2001), Plume–lithosphere interactions in the generation of the basalts of the Kenya rift, East Africa, *J. Pet.*, *42*(5), 877–900.

Maruyama, S., D. A. Yuen, and B. F. Windley (2007), Dynamics of plumes and super-plumes through time, in *Superplumes: Beyond Plate Tectonics*, edited by D. A. Yuen et al., pp. 441–502, Springer, Heidelberg, Germany.

Mathu, E., and T. Davies (1996), Geology and the environment in Kenya, *J. Afr. Earth Sci.*, *23*(4), 511–539.

Mechie, J., G. Keller, C. Prodehl, M. Khan, and S. Gaciri (1997), Structure and dynamic processes in the lithosphere of the Afro-Arabian rift system: A model for the structure, composition and evolution of the Kenya rift, *Tectonophysics*, *278*(1–4), 95–119.

Mégnin, C., and B. Romanowicz (2000), The three-dimensional shear velocity structure of the mantle from the inversion of body, surface, and higher-mode waveforms, *Geophys. J. Int.*, *143*, 709–728.

Mercier J., M. Bostock, J. Cassidy, K. Dueker, J. Gaherty, E. Garnero, J. Revenaugh, and G. Zandt (2009), Body-wave tomography of western Canada, *Tectonophysics*, *475*, 480–492.

Montelli, R., G. Nolet, F. Dahlen, and G. Masters (2006), A catalogue of deep mantle plumes: New results from finite-frequency tomography, *Geochem. Geophys. Geosyst.*, *7*, Q11007, doi:10.1029/2006GC001248.

Morley, C., W. Westcott, D. Stone, R. Harper, S. Wigger, and F. Karanja (1992), Tectonic evolution of the northern Kenya rift, *J. Geol. Soc. London*, *149*, 333–348.

Mulibo, G. D. (2012), Investigation of mantle structure beneath eastern Africa: Implications for the origin of the Cenozoic tectonism and propagation of the rift system, Ph.D. thesis, The Penn. State Univ., Univ. Park, Penn.

Mutter, J., W. Buck, and C. Zehnder (1988), Convective partial melting: A model for the formation of thick basaltic sequences during the initiation of spreading, *J. Geophys. Res.*, *93*, 1031–1048.

Neele F., J. C. VanDecar, and R. Snieder (1993), The use of P wave amplitude data in a joint inversion with travel times for upper mantle velocity structure, *J. Geophys. Res.*, *98*, 12,033–12,054.

Noble, W., D. Foster, and A. Gleadow (1997), The post-Pan-African thermal and extensional history of crystalline basement rocks in eastern Tanzania, *Tectonophysics*, *275*, 331–350.

Nyblade, A. A. (2011), The upper-mantle low-velocity anomaly beneath Ethiopia, Kenya, and Tanzania: Constraints on the origin of the African superswell in eastern Africa and plate versus plume models of mantle dynamics, in *Volcanism and Evolution of the African Lithosphere*, edited by L. Beccaluva, G. Bianchini, and M. Wilson, *Geol. Soc. Am., Spec. Paper*, *478*, 1–14, doi:10.1130/2011.2478(03).

Nyblade, A. A. and C. Langston (2002), Broadband seismic experiments probe the East African rift, *Eos Trans. AGU*, *83*(405), 408– 09.

Nyblade, A. A., C. Birt, C. Langston, T. Owens, and R. Last (1996), Seismic experiments reveals rifting of Craton in Tanzania, *Eos Trans. AGU*, *77*, 517–521.

Nyblade, A. A., T. Owens, H. Gurrola, J. Ritsema, and C. Langston (2000), Seismic evidence for a deep upper mantle thermal anomaly beneath East Africa, *Geology*, *28*, 599–602.

O'Donnell, J., A. Adams, A. A. Nyblade, G. D. Mulibo, and F. Tugume (2013), The uppermost mantle shear wave velocity structure of eastern Africa from Rayleigh wave tomography: Constraints on rift evolution, *Geophys. J. Int.*, doi:10.1093/gji/ggt135, in press.

Owens, T., A. Nyblade, H. Gurrola, and C. Langston (2000), Mantle transition zone structure beneath Tanzania, East Africa, *Geophys. Res. Lett.*, *27*(6), 827–830.

Park, Y., and A. A. Nyblade (2006), P-wave tomography reveals a westward dipping low velocity zone beneath the Kenya rift, *Geophys. Res. Lett.*, *33*, L07311, doi:10.1029/2005GL025605.

Pasyanos, M., and A. Nyblade (2007), A top to bottom lithospheric study of Africa and Arabia, *Tectonophysics*, *444*, 27–44.

Pik, R., B. Marty, and D. R. Hilton (2006). How many mantle plumes in Africa? The geochemical point of view, *Chem. Geol.*, *226*, 100–114.

Pinna, P., S. Muhongo, E. Le Goff, B. Mcharo, Y. Deschamps, J. Milesi, P. Vinauger, and F. Ralay (2004), Geology and Mineral Map of Tanzania, Scale 1:2,000,000, Geol. Surv. Fra., Orleans, France.

Priestley, K., D. McKenzie, E. Debayle, and S. Pilidou (2008), The African upper mantle and its relationship to tectonics and surface geology, *Geophys. J. Int.*, *175*, 1108–1126.

Ritsema, J., and R. Allen (2003), The elusive mantle plume, *Earth Planet. Sci. Lett.*, *207*, 1–12.

Ritsema, J., A. A. Nyblade, T. Owens, C. Langston, and J. VanDecar (1998), Upper mantle seismic velocity structure beneath Tanzania, East Africa: Implications for the stability of cratonic lithosphere, *J. Geophys. Res.*, *103*, 21,201–21,213.

Ritsema, J., H. van Heijst, and J. Woodhouse (1999), Complex shear wave velocity structure beneath Africa and Iceland, *Science*, *286*, 1925–1928.

Ritsema, J., A. Deuss, H. van Heijst, and J. Woodhouse (2011), S40RTS: A degree-40 shear-velocity model for the mantle from new Rayleigh wave dispersion, teleseismic traveltime and normal-mode splitting function measurements, *Geophys. J. Int.*, *184*, 1223–1236.

Roberts, E., N. Stevens, P. O'Connor, P. Dirks, M. Gottfried, W. Clyde, R. Armstrong, A. Kemp, and S. Hemming (2012), Initiation of the western branch of the East African Rift coeval with the eastern branch, *Nature Geosci.*, *5*, 289–294.

Sebai, A., E. Stutzmann, J. Montagner, D. Sicilia, and E. Beucler (2006), Anisotropic structure of the African upper mantle from Rayleigh and Love wave tomography, *Phys. Earth Planet. Int.*, *155*, 48–62.

Simmons, N. A., A. M. Forte, S. P. Grand (2007). Thermochemical structure and dynamics of the African superplume, *Geophys. Res. Lett.*, *34*, L02301, doi:10.1029/2006GL028009.

Simmons, N., A. Forte, and S. Grand (2009), Joint seismic, geodynamic and mineral physical constraints on three-dimensional mantle heterogeneity: Implications for the relative importance of thermal versus compositional heterogeneity, *Geophys. J. Int.*, *177*, 1284–1304.

Simmons, N., A. Forte, L. Boschi, and S. Grand (2010), GyPSuM: A joint tomographic model of mantle density and seismic wave speeds, *J. Geophys. Res.*, *115*, B12310, doi:10.1029/2010JB007631.

Simmons, N. A., S. C. Myers, G. Johannesson, and E. Matzel (2012), LLNL-G3Dv3: Global P wave tomography model for improved regional and teleseismic travel time prediction, *J. Geophys. Res.*, *117*, B10302, doi:10.1029/2012JB009525.

Slack, P., P. Davis, H. Dahlheim, A. Glahn, J. Ritter, W. Green, P. Maguire, and R. Meyer (1994), Attenuation and velocity of P-waves in the mantle beneath the East African rift, Kenya, *Tectonophysics*, *236*(1-4), 331–358.

Sobolev, S., H. Zeyen, G. Stoll, F. Werling, R. Altherr, and K. Fuchs (1996), Upper mantle temperatures from teleseismic tomography of French Massif Central including effects of composition, mineral reactions, anharmonicity, anelasticity and partial melt, *Earth Planet. Sci. Lett.*, *139*(1–2), 147–163.

Spiegel, C., B. Kohn, D. Belton, and A. Gleadow (2007), Morphotectonic evolution of the central Kenya rift flanks: Implications for late Cenozoic environmental change in East Africa, *Geology*, *35*, 427–430.

VanDecar, J. (1991), Upper mantle structure of the Cascadia subduction zone from non-linear teleseismic travel time inversion, PhD thesis, Univ. of Wash., Seattle, Wash.

VanDecar, J., and R. Crosson (1990), Determination of teleseismic relative phase arrival times using multi-channel cross-correlation and least squares, *Bull. Seismol. Soc. Am.*, *80*, 150–169.

VanDecar, J. C., D. E. James, and M. Assumpcão (1995), Seismic evidence for a fossil mantle plume beneath South America and implication for plate driving forces, *Nature*, *378*, 25–31.

Venkataraman, A., A. A. Nyblade, and J. Ritsema (2004), Upper mantle Q and thermal structure beneath Tanzania, East Africa, from teleseismic P-wave spectra, *Geophys. Res. Lett.*, *31*, L15611, doi:10.1029/2004GL020351.

Walker, K., A. A. Nyblade, S. Klemperer, G. Bokelmann, and T. Owens (2004), On the relationship between extension and anisotropy: Constraints from shear wave splitting across the East African Plateau, *J. Geophys. Res.*, *109*, B08302, doi:10.1029/2003JB002866.

Weeraratne, D., D. Forsyth, K. Fischer, and A. A. Nyblade (2003), Evidence for an upper mantle plume beneath the Tanzanian craton from Rayleigh wave tomography, *J. Geophys. Res.*, *108*(B9), 2427, doi:10.1029/2002JB002273.

Wiens, D., J. Conder, and U. Faul (2008), The seismic structure and dynamics of the mantle wedge, *Ann. Rev. Earth Planet. Sci.*, *36*, 421–455.

Yuen, D. A., M. Monnereau, U. Hansen, M. Kameyama, and C. Matyska (2007), *Dynamics of Superplumes in the Lower Mantle, in Superplumes: Beyond Plate Tectonics*, edited by D. A. Yuen et al., pp. 239–268, Springer, Heidelberg, Germany.

Zhao, D. (2004), Global tomographic images of mantle plumes and subducting slabs: Insight into deep Earth dynamics, *Phys. Earth Planet. Int.*, *146*, 3–34.